

# Adaptive Control of an Inductive Power Transfer Coupling for Servomechanical Systems

Deron K. Jackson    Steven B. Leeb    Steven R. Shaw

*Abstract*— This paper presents adaptive-control schemes that estimate load-model parameters and adaptively “tune” a digital controller for an inductively-coupled power delivery circuit. Estimation algorithms are presented that utilize specific recursive formulations, which provide adequate noise immunity in a power-electronic environment. The techniques are demonstrated using a servomechanical system and a 1.5-kW prototype power electronic drive.

## I. INTRODUCTION

IN contrast to controllers for typical regulation applications, servomechanical systems generally require a controller whose transient performance is verifiably guaranteed over a wide range of operating conditions. Also, for adequate tracking performance, the controller may need to respond relatively swiftly to command changes or load disturbances. An array of servomechanical control problems exist where slow variations (compared to control bandwidth) in mechanical properties, loading, or external disturbances lead to changes in the load model parameters. Such changes can adversely affect even relatively robust control designs.

Adaptive or “self-tuning” controls adjust automatically in response to system changes. Adaptive control systems have been widely studied [1], [2]. The name generally refers to a two step process of system parameter estimation and control adaptation. Both tasks must be accomplished on-line to permit the controller to track time-varying system parameters. This imposes certain limits on implementations. In addition, the adaptation algorithm must be suitable for digital implementation and sufficiently robust to noise. This paper addresses these concerns and presents techniques specifically suited to power electronic and digital control environments.

The authors are with the Laboratory for Electromagnetic and Electronic Systems and the Center for Materials Science and Engineering, Massachusetts Institute of Technology, Cambridge, MA 02139, USA

## II. SYSTEM OVERVIEW

A number of circuit topologies for inductively coupled power transfer in servomechanical applications are reviewed in [3]. One power electronic drive, for example, is a unidirectional power transfer coupling that draws power from the AC utility through a high power factor pre-regulator. Power is transferred to the load through a half-bridge inverter that energizes a separable transformer or inductive coupling. Another drive explored in [3] employs a high power factor pre-regulator capable of bidirectional power transfer, to or from the electric utility, and either a full-bridge or symmetric half-bridge inverter circuit capable of transferring power to or from a load through the inductive coupling.

An inductive coupling provides features including: safety isolation; a separable or sliding, non-ohmic electro-mechanical interface; and, often, the possibility of transferring power across an unbroken environmental interface, e.g., the skin of a patient receiving an externally powered *in-vivo* implant, or a wall in a transportation system. The advantages and engineering challenges of operating this type of coupling and the associated drive circuitry over a range of power levels and applications have been reviewed in numerous publications, including [4], [5], [6], [7], [8], and [9], among others.

In [10], [11], and [12], we exploited large-signal linear models for developing controllers for the inductively-coupled power electronic drives used in [3]. Large-signal linear models are essential for developing controllers with verifiable performance in tracking applications. The general multirate digital control techniques developed in [3], [12], and [11] presume that the driving-point impedance or other input-to-output behavior of the load can be described by a linear, time-invariant transfer-function model. The time invariance constraint implies that the differential equations or transfer function describing the load model contains constant coefficients. These coefficients must be known in order to apply conventional design techniques. Not surprisingly, a number of applications do not fit this description.

The next sections present techniques for estimating the slowly varying coefficients of a load model for a load driven by an inductively coupled power electronic drive. These techniques can be used to update the gains of a controller to ensure specified performance under load changes. The parameter estimation and adaptive controller demonstrations are constructed using a prototype 1.5 kW inductively coupled drive (described in detail in [3]). However, the estimation techniques could be used in virtually any on-line, digitally controlled power electronic application. Also, since many power electronic drives employ a fixed (non-separable) transformer for isolation or voltage conversion, the demonstration of these control techniques with an inductively coupled (separable transformer) drive, which is very similar to a fixed transformer drive, does not limit their applicability.

### III. PARAMETER ESTIMATION FOR POWER ELECTRONIC DRIVES

A conventional linear estimation problem begins with the assumption that a column vector  $\mathbf{y}$  composed of scalar measurements  $y[k]$  can be related to the product of a “regressor” matrix  $\mathbf{R}$  (composed of row vectors  $\mathbf{r}[k]^T$ ) and a column vector of parameters  $\boldsymbol{\theta}$  which characterize the system [2]:

$$\mathbf{R}\boldsymbol{\theta} = \mathbf{y} \quad (1)$$

In a typical application, a large number (relative to the number of parameters in  $\boldsymbol{\theta}$ ) of measurements are made to assemble the  $\mathbf{y}$  vector. The system is overconstrained. Generally, no vector  $\boldsymbol{\theta}$  can be found that precisely satisfies (1). The least-squared error solution

$$\hat{\boldsymbol{\theta}} = (\mathbf{R}^T\mathbf{R})^{-1}\mathbf{R}^T\mathbf{y} \quad (2)$$

minimizes the sum of the squared errors, i.e., the 2-norm of the vector  $\mathbf{y} - \mathbf{R}\hat{\boldsymbol{\theta}}$ . (The “hat” notation is used throughout this paper to indicate estimated quantities.) Note that direct solution of (2) is a numerically poorly conditioned approach for finding  $\hat{\boldsymbol{\theta}}$ , and that recursive formulations based on this equation may also be numerically inferior to more clever solution techniques. It is imperative to ensure that the number of parameters does not exceed the number that can be identified given the information content or “richness” of the measurements, e.g., the matrix  $\mathbf{R}$  should not be too poorly numerically conditioned. Given sufficiently rich measurements, all of these estimation approaches are generally functional for application with thriftily modeled servomechanical drives with small numbers of parameters to be estimated.

#### A. Recursive Least-Squares Estimation

Recursive least-squares (RLS) estimation is an iterative reformulation of the conventional least-squares solution technique for overconstrained linear systems [2]. Rather than waiting to accumulate a collection of measurements before estimating the parameter vector, as in conventional least-squares estimation, the estimate  $\hat{\boldsymbol{\theta}}$  can be updated as each new measurement is made. The RLS estimator is very attractive for real-time applications. Because the RLS algorithm is recursive, very few data points need to be stored between iterations, and computations occur at specified intervals with a predictable computational complexity.

The recursive least-squares algorithm is shown in (3) below:

$$\begin{aligned} \epsilon[k] &= y[k] - \mathbf{r}[k]^T\hat{\boldsymbol{\theta}}[k-1] \\ \mathbf{g}[k] &= \frac{\mathbf{P}[k-1]\mathbf{r}[k]}{\rho + \mathbf{r}[k]^T\mathbf{P}[k-1]\mathbf{r}[k]} \\ \hat{\boldsymbol{\theta}}[k] &= \hat{\boldsymbol{\theta}}[k-1] + \mathbf{g}[k]\epsilon[k] \\ \mathbf{P}[k] &= \frac{1}{\rho}(\mathbf{P}[k-1] - \mathbf{g}[k]\mathbf{r}[k]^T\mathbf{P}[k-1]) \end{aligned} \quad (3)$$

where  $\epsilon[k]$  is a scalar prediction error,  $\mathbf{g}[k]$  is a gain vector, and  $\mathbf{P}[k]$  is a weighting matrix [1]. The algorithm in (3) is executed from top to bottom at each iteration of the index  $k$ .

For now, assume that the “forgetting factor,”  $\rho$ , is unity. In this case, after  $N$  iterations, the recursive algorithm can, with infinite precision arithmetic, return the exact parameter estimates that would occur using non-recursive least squares on the same  $N$  data points. However, a perfect match requires very specific initial conditions for  $\mathbf{P}[k]$ . In practice, the matrix  $\mathbf{P}[0]$  and the initial parameter vector may be determined by producing initial estimates, perhaps offline, using conventional least squares. Alternatively, the algorithm could be started with an initial guess at the parameters and a  $\mathbf{P}[0]$  matrix set to a large constant multiplied by an identity matrix. Although this can cause large initial transients in the parameter estimate, the large  $\mathbf{P}[0]$  helps assure relatively rapid parameter convergence.

The RLS algorithm just described refines its parameter estimates at each iteration. So after  $N$  iterations the accuracy of the estimate accumulates the contributions from all  $N - 1$  previous iterations. This prevents the algorithm from accurately tracking time-varying parameters unless the effect of distant data points can somehow be mitigated. This can be accomplished by setting the forgetting factor  $\rho$  to a value less

than unity. The forgetting factor modifies the minimization criteria of the RLS algorithm so that errors that occurred at time index  $k - i$  are weighted by  $\rho^i$ . The number of samples effectively kept in “memory” is roughly proportional to  $1/(1 - \rho)$  [2].

Exponential forgetting must be tuned with some care for optimum performance. If  $\rho$  is chosen too large, it will lead to slow convergence of the estimates, and if chosen too small, it will result in noisy estimates, which are based on too few data points. Thus, the choice of  $\rho$  represents a trade-off between parameter tracking and disturbance rejection. Another problem, known as “covariance matrix explosion,” may occur during moments of low excitation [2]. In the absence of a significantly exciting input, the quantity  $\mathbf{P}[k - 1]\mathbf{r}[k]$  will approach zero, in which case  $\mathbf{P}[k]$  will begin to increase exponentially. In turn, the parameter estimates become increasingly sensitive to the prediction error  $\epsilon[k]$ , and the slightest noise or model inaccuracy can lead to erratic or erroneous parameter estimates. In practice, we could attempt to mitigate this effect by skipping the RLS update if a defined variable, such as the output, changes by less than an amount  $\delta$  between samples.

Recursive estimation is a rich topic that has received much research attention. Many modifications have been proposed to optimize the performance of the basic recursive estimator for noise environments with specific, known probabilistic distributions. Also, note that the performance analyses of the basic least squares approach typically assume that noise or measurement error is confined to the vector of observations and assumes an understood form. In fact, in servomechanical applications of interest, noise often affects both the measurement vector and the regressor matrix. Other techniques, e.g., “total” least squares [13], have been developed to provide solutions that are optimal in some sense for these cases. Generally, careful characterization of the noise environment in a power electronic servomechanism, where disturbances and noise may be closely correlated and impulsive or non-Gaussian in nature, is difficult. Experiments with the prototype hardware show that using the RLS estimation technique to determine the parameters of a “state-variable-filtered” plant model can lead to relatively noise-immune parameter estimation techniques suitable for the power electronic environment.

### B. State Variable Filtering

The term “lambda method” (LM) is used here to describe a modification to the conventional recursive

least-squares (RLS) algorithm, which will be referred to as LM-RLS. The technique relies on an “operator transformation” that allows the differentiation operator in a continuous-time (CT) transfer function model to be replaced, in principle, without approximation. The result is a discrete-time (DT) estimation algorithm, which operates on transformed or filtered observations of the input and output data. An estimation algorithm can then be designed around the transformed model. This technique is described briefly in [2] and in other literature under the heading “model transformation” or “state-variable filter”, but appears to have been largely overlooked in the power-electronics literature. However, our experiments demonstrate that a substantial reduction in noise sensitivity can be achieved in comparison to conventional RLS.

The LM-RLS technique is developed around a CT transfer function model of the system, e.g., the rational CT transfer function

$$H(s) = \frac{b_1 s^{m-1} + \dots + b_m}{s^m + a_1 s^{m-1} + \dots + a_m} \quad (4)$$

where the denominator polynomial has order  $m$  and the coefficients  $a_i$  and  $b_i$  may be time varying. This system function might model the driving point admittance of a battery to be charged, or the through transfer function of a speed-control servomechanism, or, generally, the system function of any plant to be driven and controlled by a power electronic drive. The coefficients of  $H(s)$  equivalently describe a linear differential equation model of the system written as

$$p^m y(t) + a_1 p^{m-1} y(t) + \dots + a_m y(t) = b_1 p^{m-1} u(t) + \dots + b_m u(t) \quad (5)$$

where  $p$  represents the derivative operator  $\frac{d}{dt}$  and  $u(t)$  and  $y(t)$  represent the input and output variables of the system with system function (4). An operator transformation can be applied to (5), whereby the  $p$  operator is replaced by the, causal, low-pass “lambda” operator

$$\lambda = \frac{1}{\tau_\lambda p + 1} \quad (6)$$

where  $\tau_\lambda$  is a positive time constant. Using (6) to eliminate  $p$  from (5) yields a new linear model, which can be written as

$$y(t) + \alpha_1 \lambda y(t) + \dots + \alpha_m \lambda^m y(t) = \beta_1 \lambda u(t) + \dots + \beta_m \lambda^m u(t) \quad (7)$$

where the reformulated parameters  $\alpha_i$  and  $\beta_i$  are algebraically related to the starting parameters  $a_i$ ,  $b_i$ ,



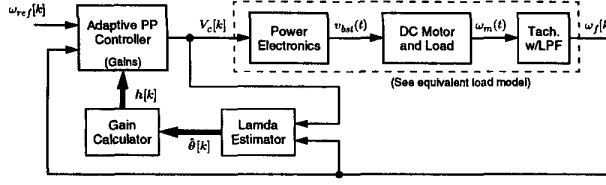


Fig. 2. Block diagram for motor speed control experiments.

noise from the tachometer voltage.

### A. Control Design

The multi-loop adaptive speed control system is illustrated in Fig. 2. The system actually consists of three nested control loops. An innermost analog loop (not shown explicitly) controls the wave-shaping provided by a unity power factor, interleaved boost pre-regulator in the power electronics block. Next, a digital loop (again hidden in the dashed box), based on a large signal linear model of the boost converter, controls the output voltage of the converter to track with command inputs  $V_c[k]$ . The output voltage of the boost converter serves as the input to a high-frequency, DC-DC, zero-voltage switched bridge converter that transfers power across a separable inductive coupling to the electromechanical load, represented overall by the dashed box in the figure. The final feedback loop, the adaptive, pole placement (PP) compensated feedback loop, regulates mechanical speed by controlling input voltage to the motor. This DT loops runs at a slower time scale than the inner voltage regulation loop. That is, many time steps of the voltage loop occur in one time step of the speed loop. The remaining blocks in Figure 2 represent the adaptive speed controller. Parameter estimation for this controller was performed using the LM-RLS algorithm.

A transfer function that relates the output filtered tachometer voltage to the input drive voltage from the boost pre-regulator can be derived with the aid of Figure 3. The DC/DC stage energizing the inductive coupling can be modeled as an ideal transformer and a series impedance  $R_d$  (representing the droop characteristic of the open loop DC/DC stage). The output voltage of the DC/DC stage drives a 1000 Watt permanent magnet DC motor. The model for this DC motor includes an armature winding resistance  $R_f$ , an armature inductance  $L_f$  and a motor back-EMF constant  $K_m$ . The motor's torque acts to rotate an inertia  $J$  against a frictional damping  $f$ . The final

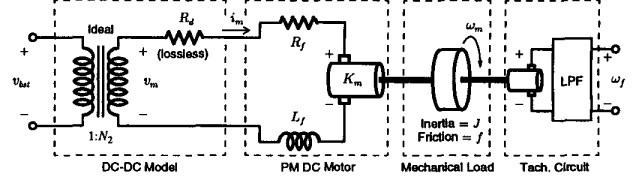


Fig. 3. Equivalent electromechanical load model.

speed of this assembly is sensed by a small tachometer mounted to the opposite end of the motor shaft. The output voltage of the tachometer is low-pass filtered to smooth out brush noise. The transfer function of this filter is

$$\frac{\Omega_f(s)}{\Omega_m(s)} = \frac{1}{\tau_f s + 1} \quad (8)$$

where the time constant  $\tau_f$  is set at approximately 10s, and  $\Omega_f(s)$  and  $\Omega_m(s)$  are the transforms of  $\omega_f(t)$  and  $\omega_m(t)$ , respectively.

The motor torque can be written as

$$T_m(t) = K_m i_m = K_m \left( \frac{N_2 v_{bst}(t) - K_m \omega_m(t)}{R_d + R_f} \right). \quad (9)$$

where the effect of the winding inductance  $L_f$  has been dropped because the armature electrical time constant is considerably shorter than the sampling interval of the DT speed controller. The load torque, which balances the motor torque, is determined by the inertia, the frictional damping, and the shaft speed:

$$T_L(t) = J \frac{d\omega_m(t)}{dt} + f \omega_m(t). \quad (10)$$

Combining (8) and the Laplace transforms of (9) and (10) yields a single CT transfer function relating the transforms of  $v_{bst}(t)$  and the tachometer speed voltage  $\omega_f(t)$ :

$$H(s) = \frac{\Omega_f(s)}{V_{bst}(s)} = \frac{g_m}{(\tau_m s + 1)(\tau_f s + 1)} \quad (11)$$

where

$$\tau_m = \frac{J}{f + \frac{K_m^2}{R_d + R_f}} \quad \text{and} \quad g_m = \frac{N_2 K_m}{f(R_d + R_f) + K_m^2}. \quad (12)$$

The inner DT voltage loop controlling the output voltage of the boost converter is designed to work quickly on the time scale of the outer DT speed loop. This means, for example, that the inner voltage loop might be configured and modeled as a ‘‘power-level’’ zero-order hold (ZOH) on the time scale of the speed loop. This configuration and other possibilities is ensured by the guaranteed dynamics of the large-signal

linear voltage loop controller with load power feed-forward discussed in [11] and [3]. Other configurations and modeling possibilities are also discussed in these references, and are exploited in this paper.

To complete the DT compensator design and determine the closed-loop system behavior, it is necessary to determine the transfer function  $\tilde{H}(z)$  for the dashed box in Fig. 2 that relates the  $z$ -transform of output speed to the  $z$ -transform of the input voltage command from the PP speed compensator. For the speed servo, we have exploited the time scale separation between the DT voltage and speed loops and the natural time constants of the plant to configure the voltage loop so that  $\tilde{H}(z)$  can be found by applying an impulse-invariant CT-to-DT transformation [14] to the transfer function  $H(s)$ :

$$\tilde{H}(z) = \frac{b_1 z}{z^2 + a_1 z + a_2} \quad (13)$$

where

$$\begin{aligned} b_1 &= \frac{g_m}{\tau_m - \tau_f} \left( e^{-\frac{T_k}{\tau_m}} - e^{-\frac{T_k}{\tau_f}} \right), \\ a_1 &= - \left( e^{-\frac{T_k}{\tau_m}} - e^{-\frac{T_k}{\tau_f}} \right), \\ a_2 &= e^{-\left( \frac{T_k}{\tau_m} + \frac{T_k}{\tau_f} \right)}. \end{aligned} \quad (14)$$

The variable  $T_k$  represents the time step of the inner voltage loop in seconds.

The impulse-invariant configuration and model for the inner voltage loop were chosen to yield an  $\tilde{H}(z)$  for which a satisfactory PP compensator could be designed. This compensator provides the beneficial property of zero steady state error without requiring an explicit DT accumulator variable. Since the load is second-order, a second-order PP compensator was developed for computing the control command  $V_c[k]$ :

$$\begin{aligned} V_c[k] &= d_1 V_c[k-1] + d_2 V_c[k-2] + h_1 (\omega_{ref}[k] - \omega_f[k]) + \dots \\ &\quad h_2 (\omega_{ref}[k] - \omega_f[k-1]) + h_3 (\omega_{ref}[k] - \omega_f[k-2]) \end{aligned} \quad (15)$$

where  $\omega_{ref}[k]$  is the motor-speed reference command and  $d_1, d_2, h_1, h_2,$  and  $h_3$  are constant gains. Saturation may be added in practice to limit the maximum and minimum voltage commands.

Combining (15) and the load model in (13) results in a closed-loop transfer function, which relates the transforms of the output tachometer voltage to the input command voltage, of the form

$$\tilde{H}_{CL}(z) = \frac{(1 + x_1 + x_2 + x_3 + x_4)z^3}{z^4 + x_1 z^3 + x_2 z^2 + x_3 z + x_4} \quad (16)$$

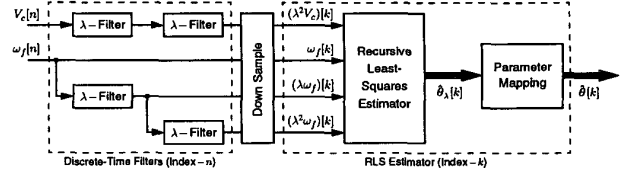


Fig. 4. Estimator.

when the control gains in (15) are related to the coefficients in the closed-loop transfer function as follows:

$$\begin{aligned} d_1 &= x_4/a_2 \\ d_2 &= d_1 - 1 \\ h_1 &= (x_1 + d_1 - a_1 + 1)/b_1 \\ h_2 &= (x_2 + d_1(a_1 - 1) + a_1 - a_2)/b_1 \\ h_3 &= (x_3 + d_1(a_2 - a_1) + a_2)/b_1. \end{aligned} \quad (17)$$

Since (17) allows the coefficients of (16) to be assigned arbitrarily, the closed-loop poles may be located freely in the  $z$ -plane. One reasonable choice for a stable, well-damped response is to place the four closed loop poles at identical locations  $m$  on the real axis, i.e.,  $z_{1,2,3,4} = m$ .

### B. Adaptive Updating

Adaptive updating of the speed controller gains is accomplished using an LM-RLS parameter estimation scheme, shown in Fig. 4. The LM-RLS estimator contains at its core an RLS estimator, which is used to estimate the parameters of a low-pass transformed system, and not the actual system. For this example, the regressor and the estimate vectors are, respectively:

$$\mathbf{r}_\lambda[k] = \begin{bmatrix} -(\lambda\omega_f)[k] \\ -(\lambda^2\omega_f)[k] \\ (\lambda^2V_c)[k] \end{bmatrix} \quad \text{and} \quad \hat{\boldsymbol{\theta}}_\lambda[k] = \begin{bmatrix} \hat{\alpha}_1 \\ \hat{\alpha}_2 \\ \hat{\beta}_2 \end{bmatrix}. \quad (18)$$

The operator symbol  $\lambda$  in (18) indicates that a particular observation is filtered. Ordinarily, a filtering operation would require that the signals are passed through an analog low-pass filter prior to being sampled. This approach is undesirable because it increases the circuit complexity. Although the filters themselves are straightforward, the number of A/D channels increases because each filtered quantity must be sampled separately. In this case four A/D channels would be required versus just two for conventional RLS.

The multirate nature of the digital control implementation provides an elegant alternative. The filtering operation can be implemented digitally at the rate

of the “fast” inner voltage loop. Since the voltage-loop time index,  $n$ , steps at a rate  $Q$  times that of the outer loop, the DT filters will appear essentially continuous on the “slow” outer-loop time scale. The transfer function of each digital “ $\lambda$ -filter” in Fig. 4 is developed by again applying a CT-to-DT transformation to the CT transfer function of a first order low-pass filter. As shown Fig. 4, the outputs are all down-sampled to the DT time index  $k$  before entering the RLS estimator block.

The output of the RLS block is a vector  $\hat{\theta}_\lambda[k]$  of parameter estimates for the transformed load model. Estimates for the coefficients of the original CT load model in (11) can be computed according to

$$\hat{\tau}_m = \frac{\hat{\beta}_2}{\hat{\alpha}_1 + \hat{\alpha}_2 + 1}, \quad (19)$$

$$\hat{\tau}_{m,f} = \frac{\tau_\lambda \hat{g}_m}{2\hat{\beta}_2} \left( 2 + \hat{\alpha}_1 \pm \sqrt{\hat{\alpha}_1^2 - 4\hat{\alpha}_2} \right).$$

The parameter estimates that are necessary to update the speed controller can be obtained from the relationships in (14) and (17). Their application yields formulas for the quantities in  $\hat{\theta}[k]$  and  $\hat{h}[k]$  below:

$$\hat{\theta}[k] = \begin{bmatrix} \hat{a}_1 \\ \hat{a}_2 \\ \hat{b}_1 \end{bmatrix} \quad \text{and} \quad \hat{h}[k] = \begin{bmatrix} \hat{d}_1 \\ \hat{d}_2 \\ \hat{h}_1 \\ \hat{h}_2 \\ \hat{h}_3 \end{bmatrix}. \quad (20)$$

The gains in  $\hat{h}[k]$  are used to update the coefficients of the control command, (15).

## V. RESULTS

The adaptive speed-control system was implemented in software on the 80C196KC microcontroller board. Detailed source listings can be found in [3]. Both fixed and adaptive controllers were implemented to allow for direct comparison. The fixed controller was optimized for operation with a load disk with a mass of 4.5 kg. The load model parameters for  $H(s)$  in (11) were approximated experimentally at this mass setting. The results were

$$\hat{\tau}_m = 11.7 \text{ s}, \quad \hat{\tau}_f = 10.0 \text{ s}, \quad \text{and} \quad \hat{g}_m = 0.011. \quad (21)$$

The closed-loop performance of both speed-control loops was targeted to have four real poles collocated at  $z = 0.70$ . A sample period for the speed loop of  $T_k = 1.0$  s was used, and the inner- and outer-loop DT step indices are related by  $n = Qk$ , where  $Q = 120$ . The LM-RLS parameter estimation for the adaptive

controller was configured with a forgetting factor  $\rho$  of 0.97. Thus, a parameter estimate is based on approximately the last 33 seconds of data. Discrete time  $\lambda$  filters were designed to approximate CT first order filters with a time constant of 10.0 seconds. In our experiments, no special initial guess was supplied for  $\hat{\theta}_\lambda[k]$ . Instead, the matrix  $\mathbf{P}$  was initialized to 10,000 times an identity matrix, and the estimates were allowed to converge on their own. In order to assure stable control during start-up, the fixed controller was engaged for the first 1.5 minutes. This allowed time for the estimates to converge before adaptive control was engaged.

Experimental results are shown in Fig. 5. The top two traces in Fig. 5 show the system under the control of the fixed compensator. The top trace shows the commanded and actual tachometer voltages. The second trace shows the commanded drive voltage. The bottom two traces in the figure show the performance of the system under adaptive PP control. The third trace again shows tachometer voltage, and the fourth shows commanded drive voltage. A square wave in speed was commanded for each of the two controllers, fixed and adaptive, in order to demonstrate the control performance. The initial load mass in the experiment was set at 4.5 kg. At this level, the closed-loop performance of both the speed controllers is nearly ideal. The step transients are consistent with the closed-loop pole locations and the tracking performance is good. The inertial mass of the system was abruptly increased at 10 minutes and again at 16 minutes into each experiment. Each increase added a 4.5 kg disk to the rotating mechanical load.

The experimental results in Fig. 5 demonstrate that the adaptive controller quickly adapts to the changing inertia of the system, and that the tracking performance remains essentially constant throughout. The fixed controller fails poorly in the face of load changes, as might be expected. The closed-loop response begins to exhibit a damped oscillatory behavior.

Each step change in the load inertia causes a definite disturbance in all three parameter estimates. In the adaptive controller, the estimates quickly converge on their new values after approximately two cycles of the step input of the system. In practice, the actual convergence time will vary depending on the excitation level of the system, the amplitude of the parameter changes, and the LM-RLS settings for  $\rho$  and  $\tau_\lambda$ . Note that the time constant  $\tau_\lambda$  of the “ $\lambda$ -filter” has an effect on the parameter convergence rate. From this perspective, an optimal setting for  $\tau_\lambda$  is equal to

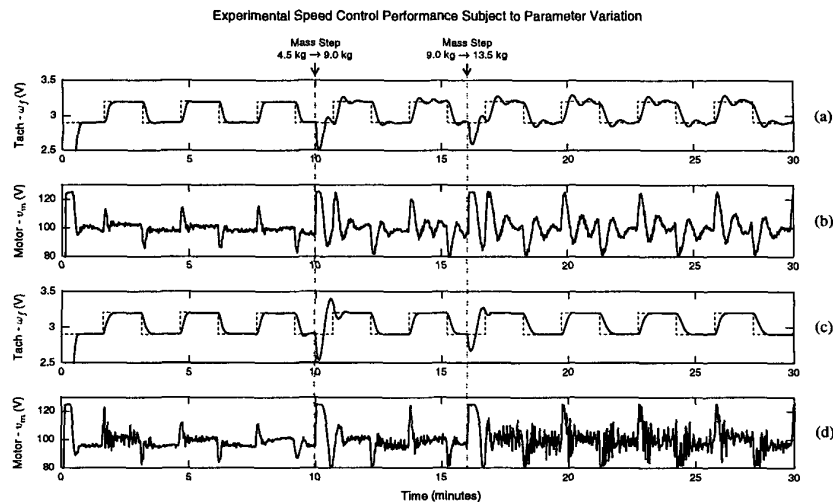


Fig. 5. Results (see text).

or slightly smaller than the time constant associated with the fastest pole in the load model. Additional consideration must be given to provide an adequate filter for the anticipated noise environment.

## VI. DISCUSSION

The performance of the LM-RLS parameter estimation proved to be superior in a high noise environment. The motor-speed control system, for example, was subject to significant electrical noise. Noise sources included brush commutation and switching spikes. Prior to the LM-RLS experiments, an adaptive motor-speed controller was implemented using direct RLS estimation. Under nearly identical conditions, the RLS estimation proved to be erratic and unreliable. The problem was traced back in part to the covariance matrix explosion described previously. It was hoped that a judicious selection of the dead-band width  $\delta$  and the forgetting factor  $\rho$  would yield satisfactory results. This was not the case. The LM-RLS method improves the situation dramatically because the regressor vector is composed of filtered measurements. Their noise content is reduced, and a much narrower dead-band  $\delta$  can be tolerated.

## ACKNOWLEDGMENTS

This research was funded by AMP, Incorporated, the National Science Foundation through a CAREER award and an MRSEC grant to the Center for Materials Science and Engineering at MIT, and MIT's Soderberg Career Development Chair. Essential hardware for this project was made available through generous donations from Intel and

Hewlett-Packard. The author's gratefully acknowledge the valuable advice and support of Mr. Joseph Sweeney, Dr. Howard Peiffer, Mr. James Wise, and Professors Jacob White, George Verghese, and Bernie Lesieutre.

## REFERENCES

- [1] G. Goodwin and K. Sin, *Adaptive Filtering Prediction and Control*, Prentice-Hall, Inc., Englewood Cliffs, NJ, 1984.
- [2] R. Johansson, *System Modeling and Identification*, Prentice-Hall, Inc., Englewood Cliffs, NJ, 1993.
- [3] D. Jackson, "Inductively Coupled Power Transfer for Electromechanical Systems," *Ph.D. Thesis*, Massachusetts Institute of Technology, May, 1998.
- [4] K.W. Klontz, A. Esser, P.J. Wolfs, and D.M. Divan, "Converter Selection for Electric Vehicle Charger Systems with a High-Frequency High-Power Link," *Power Electronics Specialists Conference*, June, 1993, pp. 855-861.
- [5] Society of Automotive Engineering, *SAE J-1773 Electric Vehicle Inductive Coupling Recommended Practice*, Warrendale, PA, February 1995.
- [6] A. Esser, "Contactless Charging and Communication System for Electric Vehicles," *IEEE Industry Applications Society Annual Meeting*, October, 1993.
- [7] N. Kutkut, K. Klontz, "Design Considerations for Power Converters Supplying the SAE J-1773 Electric Vehicle Inductive Coupler," *IEEE Applied Power Electronics Conference*, February 1997, pp. 841-847.
- [8] A.W. Kelley and W.R. Owens, "Connectorless Power Supply for an Aircraft-Passenger Entertainment System," *IEEE Transactions on Power Electronics*, Vol. 4, No. 3, July 1989, pp. 348-354.
- [9] A. Ghahary and B.H. Cho, "Design of a Transcutaneous Energy Transmission System Using a Series Resonant Converter," *IEEE Transactions on Power Electronics*, Vol. 7, No. 2, April 1992, pp. 261-269.
- [10] A.H. Mitwalli, S.B. Leeb, G.C. Verghese, and V.J. Thottuvellil, "An Adaptive Digital Controller for a Unity Power Factor Converter," *IEEE Transactions on Power Electronics*, Vol. 11, No. 2, March 1996, pp. 374-382.
- [11] D. Jackson, A. Schultz, S.B. Leeb, A. Mitwalli, G. Verghese, and S.R. Shaw, "A Multirate Digital Controller for a 1.5-kW Electric Vehicle Battery Charger," *IEEE Transactions on Power Electronics*, Vol. 12, No. 6, November 1997, pp. 1000-1006.
- [12] D. Jackson, S. Leeb, A. Schultz, and A. Mitwalli, "A Comparison of Multirate Digital Compensators for a Battery Charger," *IEEE 5th Workshop on Computers in Power Electronics*, August 1996, pp. 58 - 65.
- [13] G. H. Golub and C.F. Van Loan, "Matrix Computations," 2nd Edition, The Johns-Hopkins University Press, 1989, pp. 576-581.
- [14] K. Astrom and B. Wittenmark, "Computer Controlled Systems," Prentice-Hall, Inc., 1984.